Jurnal Teknologi

Full paper

The Effect of Inlet Air Preheat on CO and NO Production in the Combustion of Diesel in Canister Burner

Mohamad Shaiful Ashrul Ishak[a,b*], Mohammad Nazri Mohd Jaafar[b], Wan Zaidi Wan Omar[b,c]

[a]School of Manufacturing Engineering, Universiti Malaysia Perlis, P.O Box 77, Pejabat Pos Besar, 01000 Kangar, Perlis, Malaysia
[b]Department of Aeronautics, Automotive& Ocean Engineering, Faculty of Mechanical Engineering, Universiti Teknologi Malaysia, 81310 UTM Johor Bahru, Johor Malaysia
[c]Centre for Electrical Engineering System (CEES), Universiti Teknologi Malaysia, 81310 UTM Johor Bahru, Johor Malaysia

*Corresponding author: mshaiful@unimap.edu.my

Article history

Received 25 June 2014
Received in revised form 6 August 2014
Accepted 24 August 2014

Graphical abstract

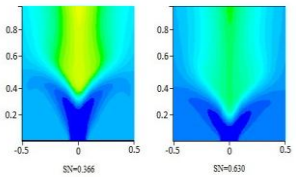

Abstract

The main purpose of this paper is to study the Computational Fluid Dynamics (CFD) prediction on the formation of carbon monoxide and oxide of nitrogen (CO-NO) inside the canister burner with inlet air pre-heating of 100 K and 250 K while varying the swirl angle of the radial swirler. Air swirler adds sufficient swirling to the inlet flow to generate central recirculation region (CRZ) which is necessary for flame stability and fuel air mixing enhancement. Therefore, designing an appropriate air swirler is a challenge to produce stable, efficient and low emission combustion with low pressure losses. A liquid fuel burner system with different radial air swirler with 280 mm inside diameter combustor of 1000 mm length was investigated. Analyses were carried out using four different radial air swirlers having 30°, 40°, 50° and 60° vane angles. The flow behavior was also investigated numerically using CFD solver Ansys Fluent. Overall results show that inlet air preheat quickens the completion of combustion such that the CO and NO production stabilized at a point nearer to fuel injection point, and reduced the CO and NO concentrations due to the combustion.

Keywords: Swirl combustion; can combustor; inlet air preheat; CFD simulation

1.0 INTRODUCTION

Swirling flow is a main flow produced by air swirled in gas turbine engine. Such flow is the combination of swirling and vortex breakdown. Swirling flow is widely used to stabilize the flame in combustion chamber [1]. Its aerodynamic characteristics obtained through the merging of the swirl movement and free vortex phenomenon that collide in jet and turbulent flow. Air swirlers are used as a flame holder by imparting swirl to the incoming air.

Swirl does not only help to stabilize the flame but also to produce other effects which are beneficial to the combustion system. These effects primarily include promoting fuel and air mixing and assisting the control of combustion temperatures and emissions. This is because of the strong shear regions, high turbulence and rapid mixing rates produced by the swirling vortices and the resulting toroidal recirculation zone. The various characteristics of swirl combustion are discussed extensively in the literatures [2-4].

The presence of swirl results in the setting up of radial and axial pressure gradients, which in turn influence the flow fields. In the case of strong swirl, the adverse axial pressure gradient is sufficiently large to generate reverse flow along the axis and generating an internal circulation zone [5-8]. In addition, swirling flows are used to improve and control the mixing process between fuel and air streams and enhance heat release rate [9].The swirl number should, if possible, should be determined from measured values of velocities and static pressure profiles. However, this is frequently not possible due to the lack of detailed experimental results. Therefore, it has been shown that the swirl number may be satisfactorily calculated from geometry of most swirl generator [9].

The geometric swirl number (S_N) has been formulated by Al-Kabie [10] and given as;

$$S_N = \frac{\sin\theta}{1 + 1/\tan\theta}\left[\frac{A_a}{C_c A_{th}}\right] \quad (1)$$

where
θ is the vane angle
A_a is the swirler exit area
A_{th} is the swirler minimum throat area
C_C is the swirler contraction coefficient

C_C is influenced by C_D and ΔP which are the swirler discharge coefficient and pressure drop respectively. Equations (2) and (3) are thus required to solve for S_N.

$$C_D = \frac{\dot{m}}{A_{th}\sqrt{2\rho\Delta P}} \quad (2)$$

where
$\dot{m}$ is the volumetric air flow rates
ΔP is the pressure drop.

$$C_C = \frac{C_D}{1+\left(\frac{C_D A_{th}}{A_a}\right)} \quad (3)$$

The swirl number should, if possible, be determined from measured values of velocity and static pressure profiles. However, this is frequently not possible due to the lack of detailed experimental results. Therefore, it has been shown that the swirl number may be satisfactorily calculated from the geometry of most swirl generator [9].

Most combustion research only report on cold air intake, whereas real combustion chamber in gas turbine engine has high temperature flow into the combustion chamber. Kelsall *et al*. reported low NO_X (5ppm) for a low flame combustion chamber, although the chamber is of high heating value (4 MJ/m^3) when fired with fuels without nitrogen [11]. In this case, the authors concluded that the flame temperature played dominant role in reducing NO_X emission. Becker *et al.* reported on combustion system development for low dry NO_X emission with high turbine inlet temperature [12]. A low emission is also reported by Dutta *et al.* in advanced recuperated engines mainly due to high combustor inlet temperature [13]. But none has really studied the effects of inlet air temperature variations on the combustion, neither on emission nor on flame development. Thus, this research focus on the investigation of the effects on air pre-heating at inlet to the formation of carbon monoxide and oxide of nitrogen (CO-NO) while varying the swirl angle inside the combustor. In this paper, the effects of the swirling flows, are studied to understand the physical processes that drives the characteristics of CO-NO formation profile, by modelling the flow using Ansys CFD software. In this study the combustion mass flow rate was assumed to be constant.

2.0 MODELING, MESHING AND BOUNDARY CONDITION

The basic geometry of the gas turbine can combustor with positions of transverse measuring stations indicated by cross section lines (z/D = 0.2 to 1.0) from the swirler throat is shown in Figure 1. The size of the combustor is 1000 mm in the Z direction, 280 mm in the X and Y direction. The primary inlet air is guided by radial curve vane swirler to give the air a swirling velocity component. Standard Ansys database of liquid diesel ($C_{10}H_{22}$) is injected at the center of swirler. Four different vane angles of 30°, 40°, 50° and 60° with the swirl numbers SN of 0.366, 0.630, 0.978 and 1.427 respectively. Based on the numerical analysis [14], the internal flows were analyzed numerically at different boundary conditions to show the effects of the swirler configurations on the turbulence production, recirculation zone and also pressure loss. The intake condition for the combustion simulation is at stoichiometry. The inlet air was supply at 300K for combustion without pre-heating and increased by 100K and 250K for two others cases.The technical data of the four swirlers used in this study are listed in Table 1.

The physical domains of the radial swirlers were decomposed to several volumes to facilitate meshing with cooper hexahedral structured grid. The geometry meshing was done to have a variable density distribution by mean of small mesh sizes which were incorporated in high gradient zone and bigger sizes in low gradient zone. The combustor model meshing for the present work is shown in Figure 2. The resulting base mesh contains approximately 0.6 million cells, which were then applied in this simulation work and presented in this paper.

In the present simulation, k-epsilon turbulence model was used. Turbulence is represented by the realizable k-epsilon model, which provides an optimal choice and economy for internal turbulent flows as suggested by [15].

The boundary conditions for this simulation are the inlet, standard wall function and the outlet as the boundaries. At the inlet of the computational region, the inlet boundary condition is defined as mass flow inlet for air supply and fuel nozzle while the exit boundary is defined as outflow. Some assumptions for boundary conditions that were not directly measured had to be made as follows:

i. Velocity components and turbulence quantities at the inlet were constant throughout the cross section;
ii. Turbulence at inlet is calculated from the following equations [16]:

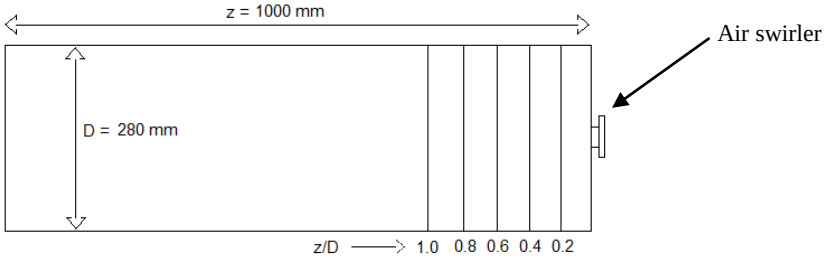

Figure 1 Details of position of transvers measuring stations indicated by cross section lines (z/D = 0.2 to 1.0) from the swirler throat

Table 1 Technical data of the swirlers

Swirler angle	30°	40°	50°	60°
Swirl No. (SN) (Based on numerical results)	0.366	0.630	0.978	1.427
Passage width, *h* (mm)	13.6	12.3	11.2	9.6
Hub diameter, *d* (mm)	50			
Outer diameter, *D* (mm)	98			

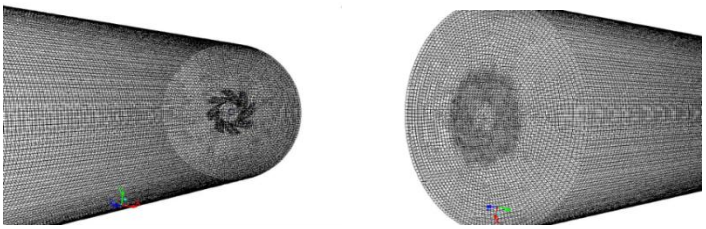

Figure 2 Combustor model meshing

$$k_{inlet} = 0.002(u^2)_{inlet} \quad (6)$$

$$\varepsilon = \frac{k_{inlet}^{1.5}}{0.3D} \quad (7)$$

where, u is the axial inlet flow velocity and *D* is the hydraulic diameter.

A collection of physical models was used to simulate the turbulent liquid fuel reacting flows. These models were selected due to their robustness and accuracy for industrial applications.

Turbulence Model: The current study uses the realizable *k–ε* turbulence model. This model is in the class of two-equation models in which the solution of two separate transport equations allows the turbulent velocity and length scales to be independently determined. The realizable *k–ε* turbulence model is robust, economic and reasonably accurate over a wide range of turbulent flow. The realizable *k–ε* turbulence model solves transport equations for kinetic energy (*k*) and its dissipation rate (*ε*). It assumes that the flow is fully turbulent, and the effects of molecular viscosity are negligible. The realizable *k–ε* turbulence model is therefore valid for fully turbulent flows, consistent with the flow characteristics in a typical combustion chamber [17].

Combustion Models: Combustion models are characterized by the type of mixing (e.g. non-premixed, premixed or partially premixed) and the reaction chemistry (e.g. finite-rate chemistry or fast chemistry). Liquid fuel combustion primarily takes place in a diffusion-limited mode (non-premixed) where fuel and oxidant are brought into contact via mixing and then react. In these types of flames, it can generally be assumed that the turbulent mixing rate is much slower than the chemical kinetics rates (fast chemistry), and hence, will be the rate-limiting step. The current study used the eddy-dissipation combustion model, which assumed that the reaction rate is controlled by the turbulent mixing rate. Hence, the turbulent mixing rate in conjunction with a global reaction mechanism is used to predict local temperatures and species profiles. This model solves the conservation equations describing convection, diffusion, and reaction sources for each component species.

*NO*x *Formation Models:* The NOx formations models used in this study include the primary NOx formation mechanisms, i.e. thermal, prompt, and fuel [18]. For thermal and prompt NOx, only the transport equation of NO is solved

$$\frac{\partial}{\partial t}(\rho Y_{NO}) + \Delta.(\rho \vec{v} Y_{NO}) = \Delta.(\rho D \Delta Y_{NO}) + S_{NO} \quad (8)$$

The transport equations are solved based on the given flow field and combustion solution. In other words, NOx is post-processed from the combustion simulation. The formation of thermal NOx is then determined by the extended Zeldovich mechanism and the rate constants for the mechanism are measured from experiments [19]. The current study also applied partial equilibrium model to predict O atom concentrations and assumed lean fuel conditions for OH formations. The prompt NOx formation depends on local fuel-to-air ratio and carbon numbers. The rate constants in the model are derived empirically for different mixing strength and fuel type [20]. The model inputs are carbon number and equivalence ratio in the combustion zone. The carbon number is 10 (diesel combustion) for volatiles and the equivalence ratio is calculated based on the actual air flow and air demand.

■3.0 RESULTS AND DISCUSSION

All the numerical results on the carbon monoxide and oxide of nitrogen (CO-NO) pollutants characteristics are presented in Figures 3 to 14. Transversal profiles of gas-phase CO-NO were obtained from the simulations at axial distances 56 mm (z/D=0.2), 112 mm (z/D=0.4), 168 mm (z/D=0.6) and 224 mm (z/D=0.8) from the swirler throat exit position. In total, four radial swirler with swirl numbers of 0.366, 0.630, 0.978 and 1.427, were investigated without air preheat and with air preheat of 100 K and 250 K.

The results show that production of oxide of nitrogen (NO) in the swirl burner is affected by the intake air temperature.

Figures 3 to 5 show that the NO concentrations in the combustion chambers increase with the increase in inlet air preheat. For the case of non-preheat, transversal profiles of total pollutant nitrogen oxide (NO) population in the liquid fuel combustor were obtained from the temperature analysis (Figure 3). The pollutant NO population was found to be well distributed across the combustor for high swirl flow but for low swirl flow this pollutants are more concentrated at the core (SN= 0.978 after z/D=0.6 and for SN=0.366 after z/D=0.8). This correlates with the flame intensity positions, where that intense heat would produce more pollutant NO [19]. In addition, for SN=0.366 the pollutant NO concentration at the combustor core near the swirler throat is very low, which can be explained by the fact that there is no flame at that point. Due to buoyancy, the flame really started at z/D=0.4, after which point the concentration pollutant NO at the core starts to increase.

The air inlets wee then preheated to 100 K and 250 K to compare with non-preheat condition. The results show that for the case of high swirl combustion (SN=1.427) at z/D=1.0, the NO concentration increased from 20 ppm without preheat to 23 ppm and 28 ppm for 100K and 250K preheat respectively. For lower swirl cases, the NO concentrations are higher for all air inlet temperatures. For SN=0.366, the NO concentrations starts at 55 ppm for inlet air without preheat, increasing to 58 ppm and 67 ppm for 100K and 250K preheat respectively. The formation of NO are presented in Figures 6 to 8 as the NO contour plots of the central axial plane. The figures also show that the maximum temperatures are increased with inlet air temperature increases; there is an overall increase in the concentration of NO by 21.8%. As the inlet temperature increases, the NO formation becomes more distributed and less peaky due to the reduction of hot spot in the chamber.

Figures 9 to 11 show the productions of carbon monoxide (CO) in the combustion chamber due to variations in inlet air preheat swirl number at different axial stations. Generally for the non-preheat case, transversal profiles of total carbon monoxide (CO) population was found to be high for low swirl combustion compared with high swirl combustion as seen in Figure 9. For high swirl flow, the CO population stabilized at short distance from the swirler throat (for SN=1.427 stabilizes at z/D=0.4). For low swirl combustion, the CO population continues to increase from the swirler throat at an average rate of 20% for every z/D of 0.2. It had not stabilized even at z/D=0.8.

Figures 9, 10 and 11 compare the CO concentrations for cases of no pre-heat, 100 K and 250 K pre-heat of the air intake. The preheat reduced the CO concentrations significantly. Taking the results for low swirl combustion, (SN=0.366 at z/D=0.8) the CO concentration decreased from 1200 ppm for inlet air without preheat, to 760 ppm and 700 ppm for inlet air of 100K and 250K preheat respectively. This comes to 41.7% of CO reduction for 250 K inlet air preheat. For higher swirl flow (SN=0.630 at z/D=0.8) the CO concentration reduces from 450 ppm without inlet air preheat to 350 ppm and 180 ppm for inlet air preheat of 100 K and 250 K respectively. This constitutes a reduction of 270 ppm (60.0%) for 250K inlet air preheat.

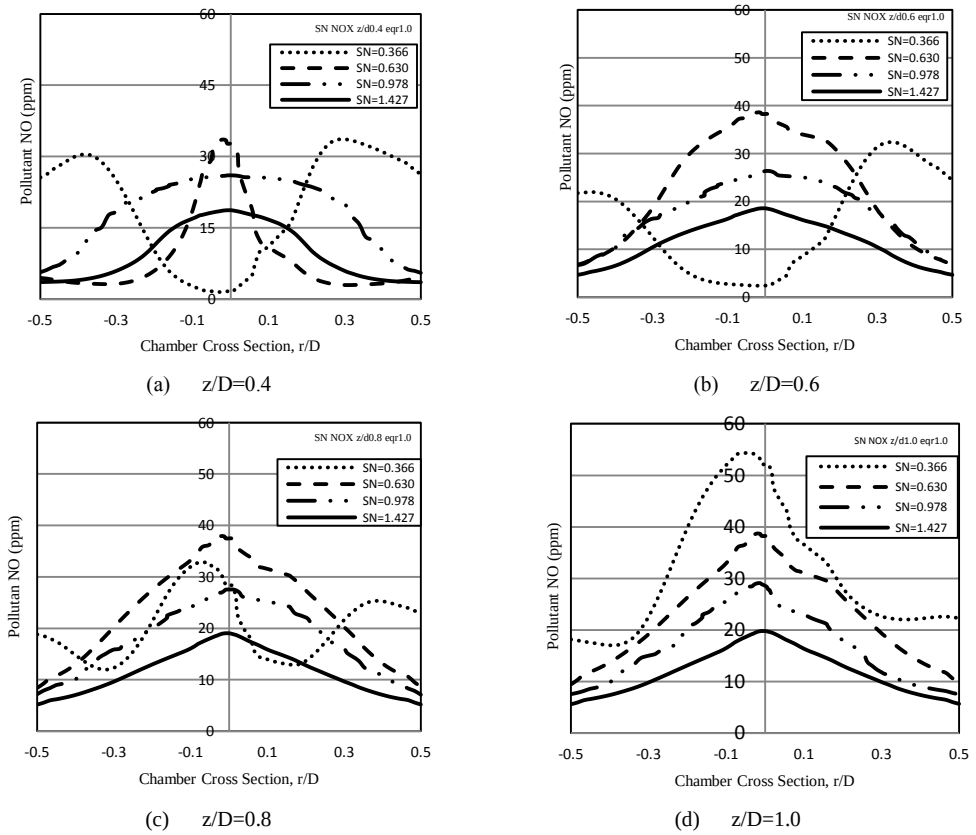

Figure 3 Transversal mean total NO Pollutant profile without pre-heat at different axial stations

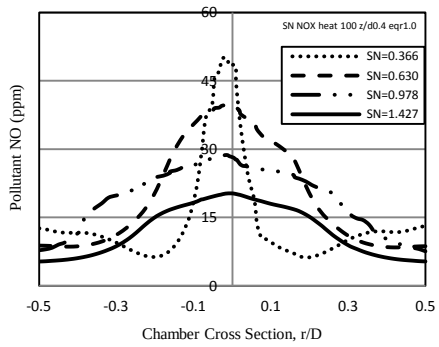

(a) z/D=0.4

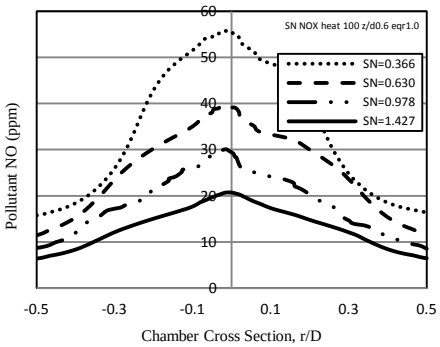

(b) z/D=0.6

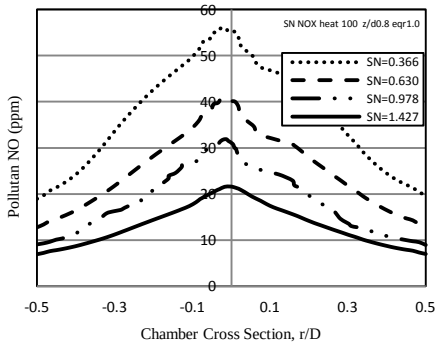

(c) z/D=0.8

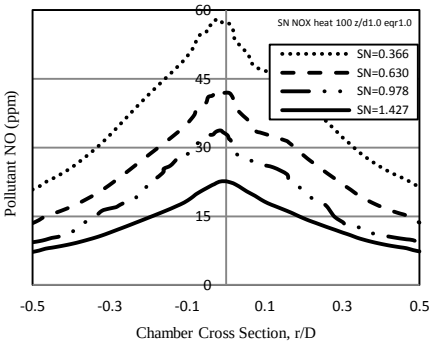

(d) z/D=1.0

Figure 4 Transversal mean total NO Pollutant profiles with 100K inlet pre-heat at different axial stations

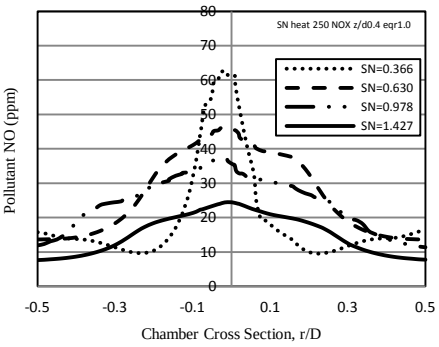

(a) z/D=0.4

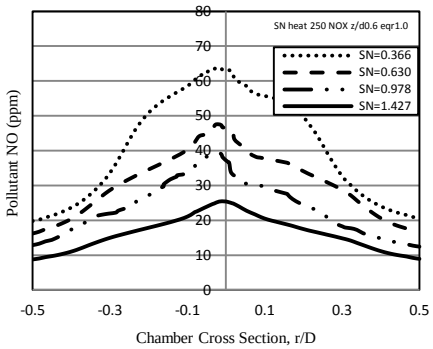

(b) z/D=0.6

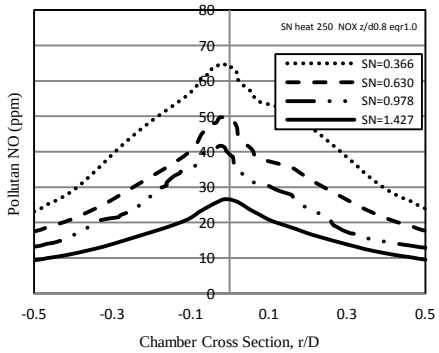

(c) z/D=0.8

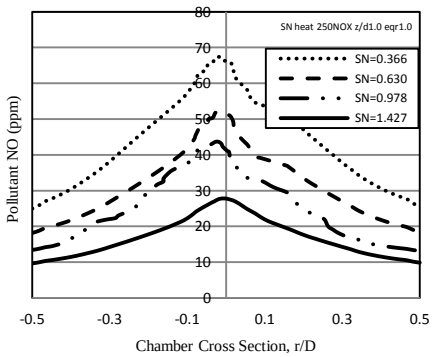

d) z/D=1.0

Figure 5 Transversal mean total NO Pollutant profiles with 250K inlet pre-heat at different axial stations

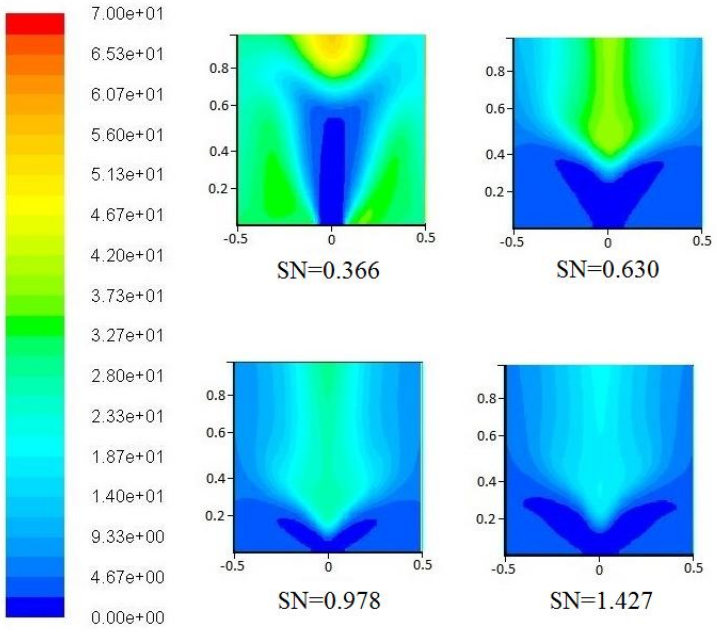

Figure 6 Total Pollutant Nitrogen Oxide (NO) Contour without pre-heat at in Axial Section of the Combustor (Scale is in ppm)

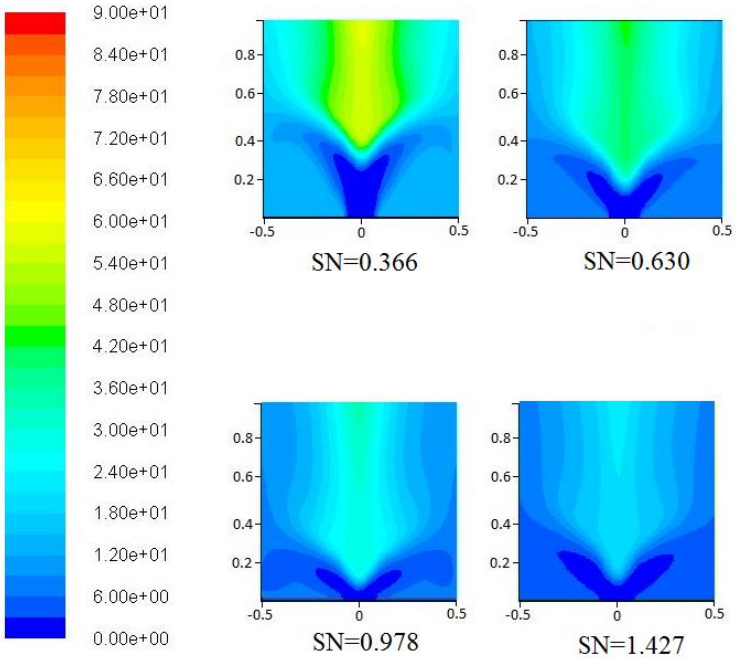

Figure 7 Total Pollutant Nitrogen Oxide (NO) Contour in Axial Section of the Combustor with 100K pre-heat (Scale is in ppm)

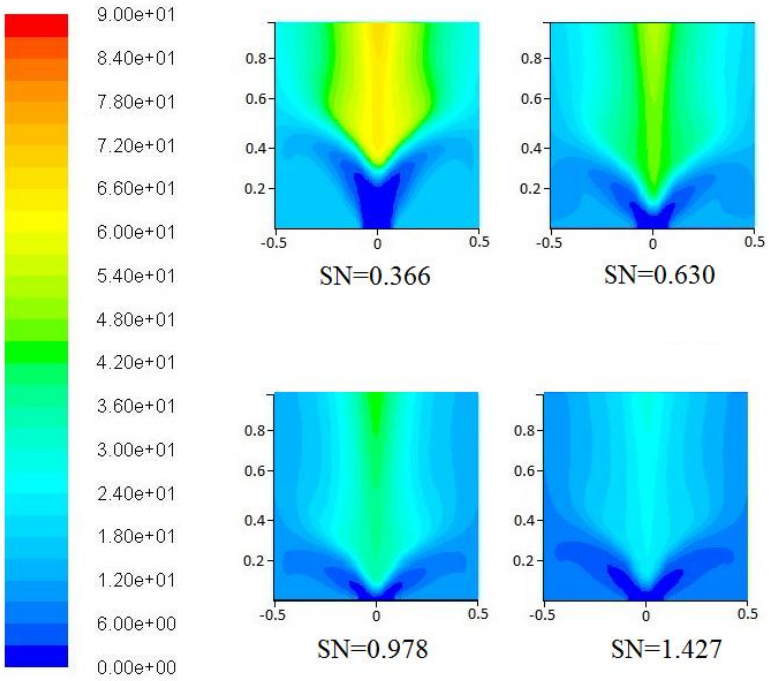

Figure 8 Total Pollutant Nitrogen Oxide (NO) Contour in Axial Section of the Combustor with 250K pre-heat (Scale is in ppm)

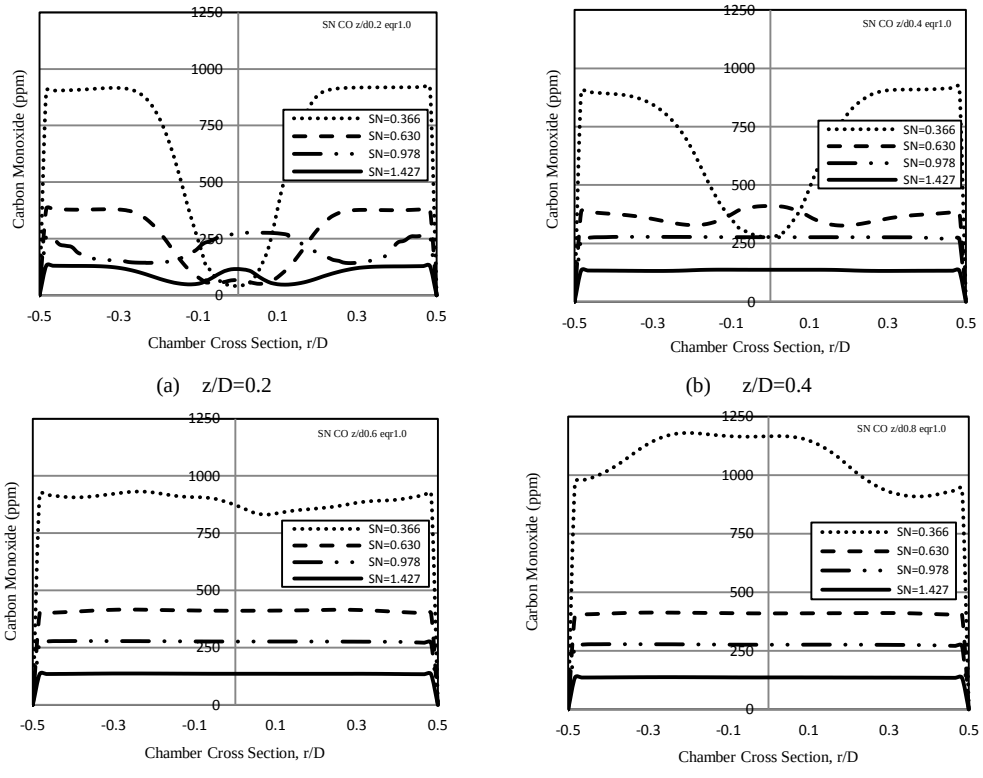

(a) z/D=0.2 (b) z/D=0.4

(c) z/D=0.6 (d) z/D=0.8

Figure 9 Transversal mean total Carbon Monoxide (CO) Pollutant profile without pre-heat at different axial stations

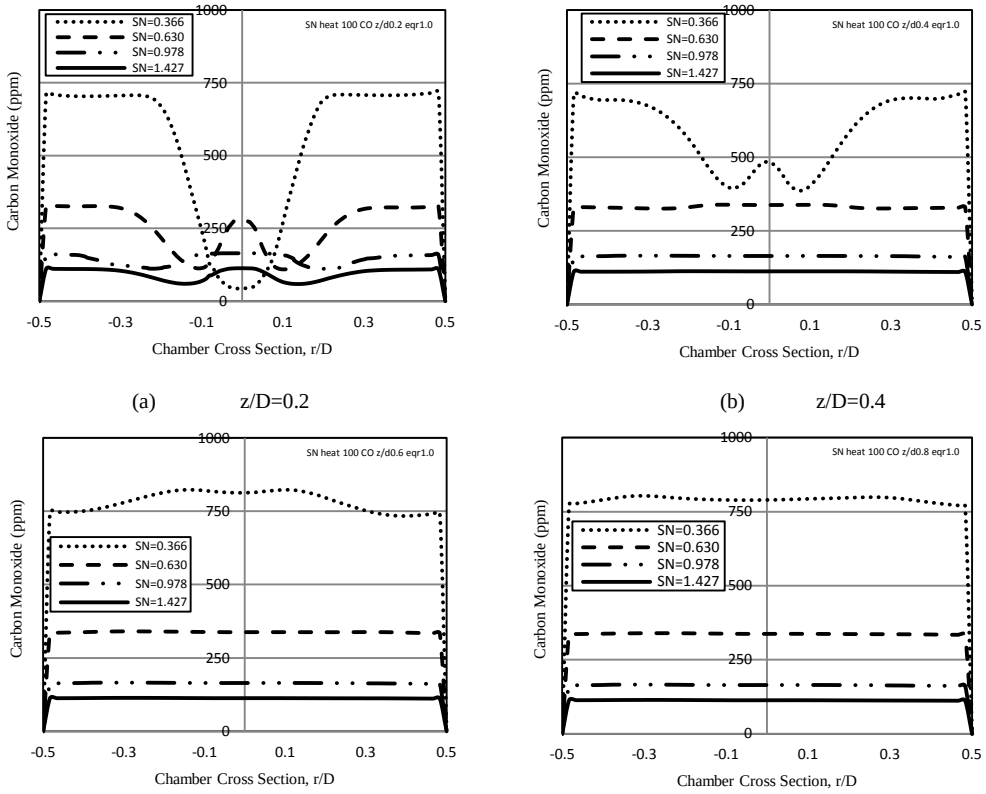

(a) z/D=0.2 (b) z/D=0.4

(c) z/D=0.6 (d) z/D=0.8

Figure 10 Transversal mean total Carbon Monoxide (CO) Pollutant profiles with 100K inlet pre-heat at different axial stations

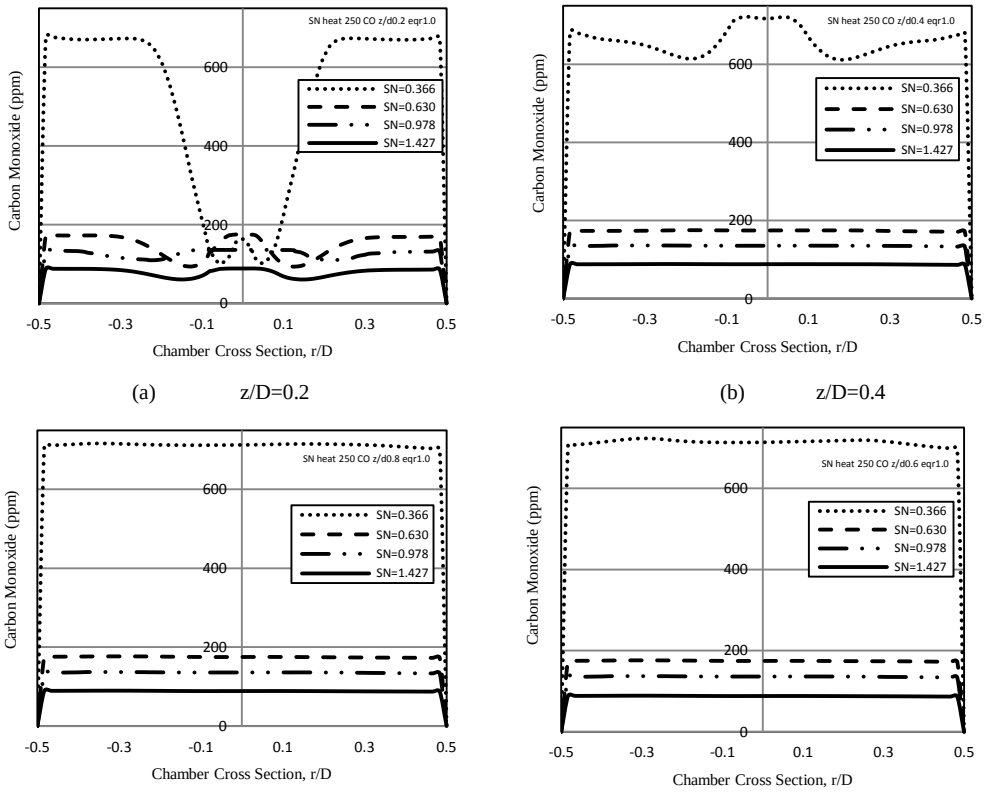

(a) z/D=0.2 (b) z/D=0.4

(c) z/D=0.6 (d) z/D=0.8

Figure 11 Transversal mean total Carbon Monoxide (CO) Pollutant profiles with 250K inlet pre-heat at different axial stations

The CO emission concentration in the chamber is also of interest. The CO concentration contours are shown in Figures 12 to 14. For low swirl combustion, without pre-heating would results in a hotspot which produce CO of up to 1200 ppm which would stabilize at z/D=0.7. When the air intake is preheated to 100K, the hotspot vanishes, and the concentration of CO came down to 800 ppm which started to stabilize at z/D=0.6. For the air intake preheat of 250K, the CO concentration further reduced to 700 ppm at z/D=0.35. For high swirl combustion, there is no hotspot for all combustions, resulting in CO concentrations to stabilize at points nearer to the fuel injection point. The CO concentration plot shows that for air intake without preheat, the CO concentration stabilized at 125 ppm at z/D=0.25, whereas for preheat of 100K and 250K, the CO concentration stabilized at 100 ppm at z/D=0.2.These results show that for high swirl combustion the CO production stabilized very quickly, stabilizing at z/D=0.25. Pre-heating the inlet air quickens CO production, stabilizing at z/D=0.20.

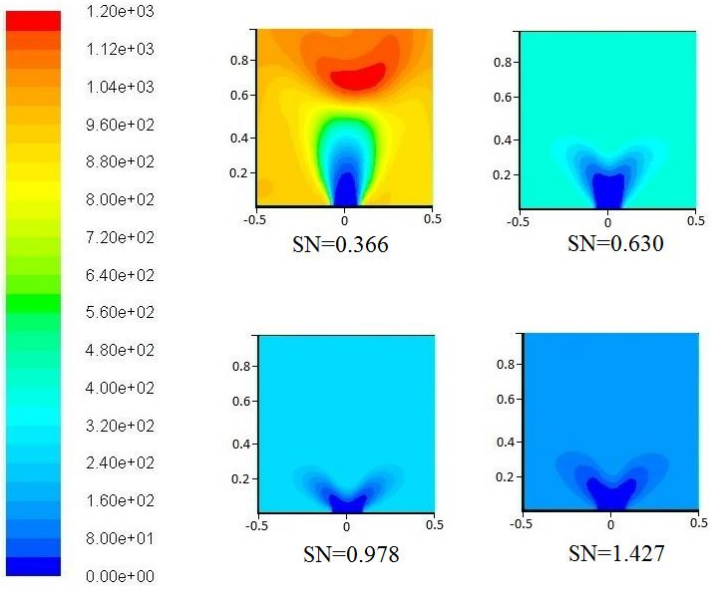

Figure 12 Total Carbon Monoxide (CO) Contour without pre-heat at in Axial Section of the Combustor (Scale is in ppm)

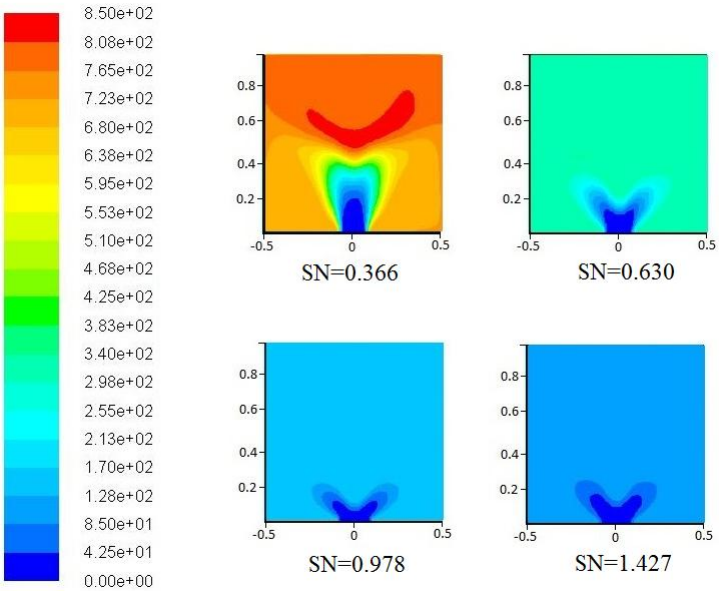

Figure 13 Total Carbon Monoxide (CO) Contour in Axial Section of the Combustor with 100K pre-heat inlet air (Scale is in ppm)

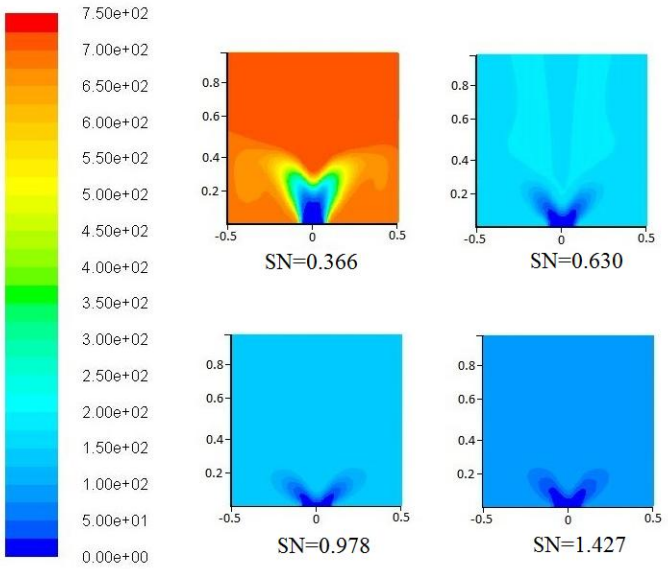

Figure 14 Total Carbon Monoxide (CO) Contour in Axial Section of the Combustor with 250K pre-heat inlet air (Scale is in ppm)

■4.0 CONCLUSION

The CFD simulation described in this paper shows that the swirl combustion with inlet air pre-heat results in improved CO-NO emission production. The CO concentration improved from 1200 ppm for combustion without inlet air pre-heat and low swirl to 100 ppm for combustion with 250 K inlet air pre-heat and high swirl combustion. Although the NO concentration due to inlet air pre-heat did improve, but the quantum of the improvement is not very significant.

Acknowledgement

The authors would like to thank the Ministry of Higher Education of Malaysia & Research Management Center, Universiti Teknologi Malaysia (project number: 01G60) for the research grant to undertake this project. The authors would also like to thank the Faculty of Mechanical Engineering, UniversitiTeknologi Malaysia for providing the research facilities and space to undertake this work.

References

(1) M.N.M. Jaafar, M.S.A. Ishak and S. Saharin. 2010. Removal of NOx and CO from a Burner System. *Environmental Science and Technology*. 44(8): 3111–3115.
(2) A.K. Gupta, D.G. Lilley and N. Syred. 1984. *Swirl Flows*. Abacus Press. Tunbridge Wells, England.
(3) D.G. Sloan, P.J. Smith, and L.D. Smoot. 1986. Modelling of Swirl in Turbulent Flow System. *Prog. Energy Combust. Sci*. 12: 163–250.
(4) M.S.A. Ishak, and M.N.M. Jaafar. 2014. Experimental Study on the Production of CO-NO-HC Emissions in the Radial Swirling Flow Combustion System. *Jurnal Teknologi*. 69(2): 45–48.
(5) A.H. Lefebvre. 1983. *Gas Turbine Combustion*, First edition. Hemisphere Publishing Corporation.
(6) A.M. Mellor. 1990. *Design of Modern Gas Turbine Combustor*. Academic Press.
(7) M.N. Mohd Jaafar, Y.A. Eldrainy, and M.F. Ahmad. 2009. Investigation of Radial Swirler Effect on Flow Pattern inside Gas Turbine Combustor. *Modern Appl. Sci.* 3(5): 21–30.
(8) A.E. Yehia, S.A. Hossam, M.S. Khalid and M.N. Mohd Jaafar. 2010. A Multiple Inlet Swirler for Gas Turbine Combustors. *Int. J. Mechanical Syst. Sci. Eng.* 2(2): 106–109.
(9) J.M. Beer and N.A. Chigier. 1972. *Combustion Aerodynamics.* Applied Science Publishers Ltd., London.
(10) H. S. Al-Kabie. 1989. *Radial Swirlers for Low Emissions Gas Turbine Combustion*. University of Leeds, Dept. of Fuel & Energy: PhD.
(11) G. J. Kelsall, M. A. Smith, and M. F. Cannon. 1994. Low emissions combustor development for an industrial gas turbine to utilize LCV fuel gas. *Journal of Engineering For Gas Turbines And Power*. 116(3): 559–566.
(12) B. Becker, W. Schulten, and B. Schetter. 1996. Combustion system development for dry low-NOx emission and high turbine inlet temperatures. *American Society of Mechanical Engineers (Paper)*. 1–6.
(13) P. Dutta, J. P. Gore, and P. E. Sojka. 1997. Emissions characteristics of liquid-fueled pilot stabilized lean premixed flames in a tubular premixer-combustor. *Journal of Engineering For Gas Turbines And Power*. 119(3): 585–590.
(14) M.S.A. Ishak, and M.N.M. Jaafar. 2014. Effect of Swirl Strength to Axial Flow Development Inside the Can Combustor. *International Review of Mechanical Engineering*. 8(1): 241–250.
(15) Y.M. Kim and T.J. Chung. 1989. Finite- Element Analysis of Turbulent Diffusion Flames. *AIAA J.* 27(3): 330–339.
(16) H.K. Versteeg and W. Malalasakera. 1995. *An Introduction to Computational Fluid Dynamics, the Finite Volume Method*. Longman Group Ltd.
(17) B. Yilmaz, S. Ozdogan, and I. Gökalp. 2008. Numerical Study on Flame-Front Characteristics of Conical Turbulent Lean Premixed Methane/Air Flames. *Energy & Fuels*. 23(4): 1843–1848.
(18) A.E. Khalil and A.K. Gupta. 2011. Distributed swirl combustion for gas turbine application. *Applied Energy*. 88(12): 4898–4907.
(19) P.T. King, G.E. Andrews, M.M. Pourkashanian, and A.C. McIntosh. 2012. Nitric Oxide Predictions for Low NOx Radial Swirlers With Central Fuel Injection Using CFD. In *ASME Turbo Expo 2012: Turbine Technical Conference and Exposition.* 985–993. American Society of Mechanical Engineers.
(20) W. Zhou, D. Moyeda, R. Payne, and M. Berg. 2009. Application of numerical simulation and full scale testing for modeling low NO_X burner emissions. *Combustion Theory and Modelling*. 13(6): 1053–1070.